Stable Path-Following Control for a Quadrotor Helicopter Considering Energy Consumption

Daniel C. Gandolfo, Lucio R. Salinas, *Member, IEEE*, Alexandre Brandão, *Member, IEEE*, and Juan M. Toibero

***Abstract*— A substantial interest in aerial robots has grown in recent years. However, the energetic cost of flying is one of the key challenges nowadays. Rotorcrafts are heavier-than-air flying machines that use lift generated by one or several rotors (vertically oriented propellers), and because of this, they spend a large proportion of their available energy to maintain their own weight in the air. In this brief, this concept is used to evaluate the relationship between navigation speed and energy consumption in a miniature quadrotor helicopter, which travels over a desired path. A novel path-following controller is proposed in which the speed of the rotorcraft is a dynamic profile that varies with the geometric requirements of the desired path. The stability of the control law is proved using the Lyapunov theory. The experimental results using a real quadrotor show the good performance of the proposed controller, and the percentages of involved energy are quantified using a model of a lithium polymer battery that was previously identified.**

***Index Terms*— Energy consumption, kinematic model, path-following controller, quadrotor, unmanned aerial vehicles (UAVs).**

I. Introduction

NOWADAYS, the advent of unmanned aerial vehicles (UAVs) is unquestionable. They have become increasingly popular in both academia and industry because of their wide range of applications, e.g., environment monitoring, safety, search and rescue, border surveillance, geology and mining, agriculture industry, or traffic control. Among the many UAVs developed in recent years, a significant focus has been placed on rotorcrafts machines because of their abilities to hover and to takeoff and land vertically. In particular, small quadrotor UAVs equipped with electric motors and fixed-pitch propellers gained popularity because of their compact size, low cost, and the ability to operate safely in any environment or in the presence of humans [1]. Besides, compared with traditional rc helicopters, quadrotors are simpler in mechanical composition. A quadrotor typically has a rigid frame with four motors, one at each end, with one propeller directly mounted on each motor without any complex transmission mechanism in between [2]. As can be seen in [3], rotorcrafts have excellent performance on different key features, such as controllability, stationary flight, low speed flight, and vertical takeoff and landing, among others; but their energy consumption is very high. In this context, it is where the motivation for this brief appears. The energetic cost of flying is one of the current key challenges, and often the reason why the missions assigned to these UAVs are impossible to complete.

In terms of control strategies, the problem of trajectory tracking is subject to limitations imposed by the nonminimum phase zeros of certain systems (such as an aircraft). The path-following approach, instead, is not subject to these limitations, because the reference is not parameterized in time, and the speed at which the path is traversed remains as an extra degree of freedom [4]. For this reason, the study of path-following techniques is an appropriate and motivating approach when considering energy consumption, since it allows the use of navigation speed as an adjustment parameter.

Several approaches for rotorcraft motion control have been developed using techniques as varied as fuzzy logic [5], predictive control [6], neural networks [7], linear quadratic regulator theory [8], Lyapunov theory [9], [10], sliding mode control [11], or linear algebra [12], among others.

Many path-following controllers have been reported in recent years for rotorcraft quadrotors. For instance, Akhtar *et al.* [13] propose a smooth, dynamic feedback controller for a quadrotor helicopter using the concepts of transverse feedback linearization and dynamic extension. Similarly, in [14], a nonlinear state feedback controller is presented; the global convergence to zero of the path-following errors is also demonstrated. Considering various control techniques, [15] presents a flight control of an autonomous quadrotor helicopter based on fuzzy sliding mode control using backstepping approach. Hernandez *et al.* [16] describe the process of identification and closed-loop control of a quadrotor as well as a path-following application based on internal model control position controllers, and then, compare it against a classic PID controller. Differential flatness-based method is addressed in [17] for controlling a quadrotor along a desired vector field, whereas [18] presents an overview on the existing works on fault detection and diagnosis and fault-tolerant control for the unmanned rotorcraft systems.

In some cases, a minimization of the control actions is proposed, such as in [19]–[21], where the control of the rotorcraft is commanded by minimizing a performance index that considers control efforts among other parameters. Moreover, in [22], a comparison of three control techniques for

Manuscript received February 15, 2016; revised May 2, 2016 and June 30, 2016; accepted August 8, 2016. Date of publication August 31, 2016; date of current version June 9, 2017. Manuscript received in final form August 9, 2016. This work was supported in part by INAUT, Universidad Nacional de San Juan, CONICET, and in part by AC3E, Universidad Técnica Federico Santa María under Grant FB0008, CONICYT. Recommended by Associate Editor L. Marconi.

D. C. Gandolfo, L. R. Salinas and J. M. Toibero are with the Consejo Nacional de Investigaciones Científcas y Técnicas, Instituto de Automática, Universidad Nacional de San Juan, San Juan J5400ARL, Argentina (e-mail: dgandolfo@inaut.unsj.edu.ar; lsalinas@inaut.unsj.edu.ar; mtoibero@inaut.unsj.edu.ar).

A. Brandão is with the Departamento de Engenharia Elétrica, Universidade Federal de Viçosa, Viçosa 36570-900, Brazil (e-mail: alexandre.brandao@ufv.br).

Color versions of one or more of the figures in this paper are available online at http://ieeexplore.ieee.org.

Digital Object Identifier 10.1109/TCST.2016.2601288

quadrotor stabilization (nested saturations, backstepping, and sliding modes) is presented, concluding that nested saturation controller should be considered as the best option in terms of lower energy consumption, because it has the minimum control action values. Another point of view is given in [23], where mechanical changes in the quadrotor are proposed to allow a terrestrial navigation; this way, the vehicle can travel longer distances under appropriate ground conditions.

In the literature discussed earlier, many controllers are based on the UAV kinematic model, and their optimal performance is shown, in general, by simulation results only. These reported results consider neither the dynamic effects that exist in real applications nor how to couple the controller to a real aircraft. However, there are also many controllers based on the dynamic model of a quadrotor, which contemplate these dynamic effects. The main disadvantage of these controllers is their inflexibility to be used in other types of UAVs. Nevertheless, in all the cases, the primary objective is to follow a desired reference path with bounded position errors, but the energy consumption and total flight time are not taken into account. In some instances, we proposed as a secondary objective to minimize the control actions; but there is not a concise idea of the real energy savings or extra navigation time achieved, because the relationship between control efforts and actual energy consumption (the energy supplied by the batteries in the case of electric propulsion) is not thoroughly studied.

This brief analyzes the influence of the velocity command over the quadrotor LiPo battery. First, the relationship between energy consumption and quadrotor speed is experimentally established. For this purpose, we consider the dynamic model of a lithium polymer battery previously identified in [24]. Thus, the results can be analyzed based on real energy consumption instead of control efforts. Next, a novel design of a kinematic path-following controller is presented and its stability is proved using the Lyapunov theory. The experimental results demonstrate how, by selecting a dynamic velocity profile, which considers path curvature as a way to penalize the speed, the path-following errors can be reduced obtaining real-world energy savings at the same time.

In this brief, it is assumed that the reference path is a requirement previously imposed, and it must be followed in the best possible way (energetically speaking); for this reason, no path planning proposal is presented.

This brief is organized as follows. Section II is devoted to the experimental justification of the relationship between speed and power consumption for a quadrotor. Section III describes the proposal for the path-following controller. Section IV explains the inclusion of path curvature to adjust the desired velocity over the path. Section V addresses the coupling between the kinematic controller and the physical UAV as a prelude to the presentation of several experimental results in Section VI. Finally, the presented approach is discussed in Section VII, and this brief is concluded in Section VIII.

II. Relationship Between Speed and Power Consumption for a Quadrotor

Unlike ground vehicles, the UAVs never stop consuming energy, because they must maintain their own weight in the air the entire time. This is even more critical in rotary-wing UAVs, since they do not have enough wing surfaces providing a lift phenomenon (as in fixed-wing UAVs), and all the thrust must be generated by the propulsion system. Then, a way to save energy in quadrotors is minimizing time aloft. In consequence, the aircraft has to move as fast as possible. However, if the quadrotor moves faster, a loss of lift is produced due to a greater inclination of its rigid body. This requires more effort from the propulsion system to generate the same weight component in the vertical axis, allowing the quadrotor to remain with the same altitude. This is shown in Fig. 1, where E and E' are the thrust generated by the propellers in hover and forward flight, respectively, being $E' > E$.

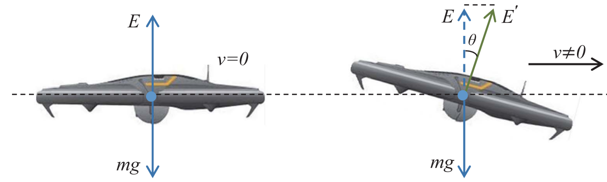

Fig. 1. Quadrotor in hover (left) and with forward speed (right).

On the other hand, in forward flights, the power requirement can be higher as the rotors torque increases to overcome parasitic drag (incurred as a result of the nonlifting surfaces, which include drag arising from the airframe, motors, and the guidance and control system at the center of the airframe). This parasitic drag is significant at high speeds for full-sized rotorcraft and becomes the predominant resistant force; for the flight envelope of quadrotor vehicles flying at moderate speeds up to 10 m/s, parasitic drag may often be ignored [25].

So, at this stage, the following questions arise. Can the loss of lift (that demands more energy) counteract the energy savings achieved by the quadrotor when it navigates a certain path faster to maintain its weight less time in the air? Do the energy savings obtained with the increase of the quadrotor speed have a significant value?

To answer these questions, the following experiment is designed: given a four-rotor helicopter AR. Drone 2.0[1] (micro UAV category with 380 g of weight and running speed of 5 m/s in perfect conditions) with GPS, it is considered its navigation over a straight path of 500 m at three different speeds $v_1 < v_2 < v_3$. In this case, the quadrotor is controlled by the application provided by the manufacturer running on a smartphone or tablet. Fig. 2(a) shows the experiment setting and Fig. 2(b) shows a photo of the flight path that has been recorded using the GPS data.

In a first experiment, three identical lithium polymer batteries, designated as B1, B2, and B3 (11.1 V and 1050 mAh), modeled in our previous work [24], were used as energy sources. At the end of each flight, the state of charge (SOC) of each battery was computed using its dynamic model. Afterward, batteries were recharged at the same initial conditions and a second experiment was made exchanging the assigned speeds to each battery to reinforce the experimental results. Table I shows the results of both the experiments.

[1] Parrot AR. Drone 2.0. http://ardrone2.parrot.com/

(a) (b)

Fig. 2. (a) AR. Drone 2.0 in the environment of the experiment. (b) Top view of the flight path provided by the GPS data.

TABLE I

ENERGY ACTUALLY CONSUMED BY THE QUADROTOR WHEN NAVIGATING AT DIFFERENT SPEEDS OVER A 500-m STRAIGHT PATH

	Battery	**Time** $[s]$	**Mean Speed** $[m/s]$	**Consumed Energy** $[\%]$
First Experiment	B1	360	1.38	50
	B2	190	2.63	30
	B3	140	3.57	22
Second Experiment	B2	357	1.4	51
	B3	185	2.7	32
	B1	138	3.62	21

It can be seen from Table I that the results are consistent. There is a difference of $\sim$29% in the consumed energy for the same distance traveled at different speeds (v_1 and v_3) exposing the quadrotor speed impact over the battery SOC and how this can motivate the study of control techniques that allow to use this extra degree of freedom (speed) with the aim of saving energy. Based on these results, Section III describes the proposed path-following controller.

III. PATH-FOLLOWING CONTROLLER

We consider the simplified kinematic model of a UAV [26], which assumes null the roll and pitch angles

$$\dot{\mathbf{x}} = \begin{bmatrix} \dot{x}_a \\ \dot{y}_a \\ \dot{z}_a \\ \dot{\psi}_a \end{bmatrix} = \begin{bmatrix} \cos(\psi_a) & -\sin(\psi_a) & 0 & 0 \\ \sin(\psi_a) & \cos(\psi_a) & 0 & 0 \\ 0 & 0 & 1 & 0 \\ 0 & 0 & 0 & 1 \end{bmatrix} \begin{bmatrix} v_{\mathrm{ax}} \\ v_{\mathrm{ay}} \\ v_{\mathrm{az}} \\ \omega_{\mathrm{az}} \end{bmatrix} = \mathbf{Ju}. \tag{1}$$

This model has only four degrees of freedom and relates linear and angular velocities in a reference frame fixed to the body of the aircraft $\mathbf{u} = [v_{\mathrm{ax}}\ v_{\mathrm{ay}}\ v_{\mathrm{az}}\ \omega_{\mathrm{az}}]^T$ with those in the inertial reference frame $\dot{\mathbf{x}} = [\dot{x}_a\ \dot{y}_a\ \dot{z}_a\ \dot{\psi}_a]^T$, being ψ_a the aircraft yaw angle and $\mathbf{J}$ the Jacobian matrix relating them.

The objective of the path-following problem is to obtain the control action $\mathbf{u_c} = [v_{\mathrm{axc}}\ v_{\mathrm{ayc}}\ v_{\mathrm{azc}}\ \omega_{\mathrm{azc}}]^T$, which allows the UAV to follow an adequate predefined path in $\Re^3$ at desired velocities and yaw angle. Then, given a geometric path $P \in \Re^3$, the intention is to find a continuous control action $\mathbf{u_c}$ such that the airship meets the following goals.

1) The rotorcraft asymptotically converges to the path P or $\lim_{t\to\infty} \tilde{\mathbf{x}}(t) = 0$; being $\tilde{\mathbf{x}} = \mathbf{x_r} - \mathbf{x}$, $\mathbf{x}$ the aircraft position and orientation vector and $\mathbf{x_r} = [x_r\ y_r\ z_r\ \psi_r]^T$ a vector formed by the point of minimum distance between P and the aircraft and desired orientation at that point.
2) The velocity $V_a = (v_{\mathrm{ax}}^2 + v_{\mathrm{ay}}^2 + v_{\mathrm{az}}^2)^{1/2}$ asymptotically converges to a desired V_d or $\lim_{t\to\infty} V_a(t) = V_d(t) > 0$.

A. Control Law

The following control action $\mathbf{u_c}$ is proposed:

$$\mathbf{u_c} = \mathbf{J}^{-1}[\mathbf{K_s} \tanh(\mathbf{K}\tilde{\mathbf{x}}) + \mathbf{v_d}] \tag{2}$$

where $\mathbf{J}^{-1}$ is the inverse of $\mathbf{J}$ (1).

In (2), tanh is the hyperbolic tangent function operating elementwise; $\mathbf{K_s} = \mathrm{diag}(k_{\mathrm{sx}}, k_{\mathrm{sy}}, k_{\mathrm{sz}}, k_{s\psi})$ and $\mathbf{K} = \mathrm{diag}(k_x, k_y, k_z, k_\psi)$ are two positive constant diagonal matrices, selected to limit the maximum value of the control action and to modify the hyperbolic tangent mapping of the position and orientation error vector, respectively. $\mathbf{v_d}$ is the desired velocity vector

$$\mathbf{v_d} = \begin{bmatrix} v_{dx} \\ v_{dy} \\ v_{dz} \\ \omega_{dz} \end{bmatrix} = \begin{bmatrix} V_d \cos(\varphi_r)\cos(\theta_r) \\ V_d \cos(\varphi_r)\sin(\theta_r) \\ V_d \sin(\varphi_r) \\ 0 \end{bmatrix} \tag{3}$$

$$\theta_r = \mathrm{atan2}(\Delta_{y_r}, \Delta_{x_r}), \quad \varphi_r = \arctan\left(\frac{\Delta_{z_r}}{\sqrt{\Delta_{x_r}^2 + \Delta_{y_r}^2}}\right)$$

where atan2 is the four quadrant arctangent function, θ_r represents the direction of the path tangent vector at (x_r, y_r, z_r) (point of minimum distance between the path and the aircraft) projected on the XY plane, and φ_r represents the elevation angle measured from the XY plane to the path tangent vector.

Remark 1: It is important to note that $\mathbf{v_d}$ and $\dot{\mathbf{x}}_r$ are not always equal. This is because $\mathbf{x_r}$ is not an external reference but depends on the actual quadrotor position (minimum-distance criterion). Therefore, if a position error exists ($\tilde{\mathbf{x}} \neq \mathbf{0}$), then, $\mathbf{x_r}$ will move on the path but with a velocity that is different to that of the aircraft ($\mathbf{v_d}$) [27]. Consequently, $\mathbf{v_d}$ and $\dot{\mathbf{x}}_r$ will be equal only when $\tilde{\mathbf{x}} = \mathbf{0}$ and the desired orientation ψ_r is equivalent to the direction of the path tangent vector θ_r.

B. Stability Analysis

Theorem 1: A quadrotor modeled by (1) follows a given geometric path $P \in \Re^3$ at a desired velocity $V_d > 0$ satisfying conditions 1) and 2) if, assuming perfect velocity tracking, i.e., $\mathbf{u} \equiv \mathbf{u_c}$, the control actions are defined by (2).

Proof: Considering the hypothesis of perfect velocity tracking, i.e., $\mathbf{u} \equiv \mathbf{u_c}$, (2) can be substituted into the kinematic model (1) to obtain the following closed-loop equation:

$$\begin{aligned} \dot{\mathbf{x}} &= \mathbf{J}\mathbf{J}^{-1}\mathbf{y} = \mathbf{K_s}\tanh(\mathbf{K}\tilde{\mathbf{x}}) + \mathbf{v_d} \\ \mathbf{0} &= (\mathbf{v_d} - \dot{\mathbf{x}}) + \mathbf{K_s}\tanh(\mathbf{K}\tilde{\mathbf{x}}). \end{aligned} \tag{4}$$

In general, the desired velocity vector $\mathbf{v_d}$ is different from the time derivative of the desired location $\dot{\mathbf{x}}_r$, and so, defining the velocity difference vector $\boldsymbol{\delta} = \dot{\mathbf{x}}_r - \mathbf{v_d}$, (4) can be written as

$$\dot{\tilde{\mathbf{x}}} + \mathbf{K_s}\tanh(\mathbf{K}\tilde{\mathbf{x}}) = \boldsymbol{\delta}. \tag{5}$$

Note that the linear velocity components of $\mathbf{v_d}$ and $\dot{\mathbf{x}}_r$ are collinear (tangent to the path).

Now, to prove the stability of the equilibrium point $\tilde{\mathbf{x}} = [\tilde{x}\ \tilde{y}\ \tilde{z}\ \tilde{\psi}]^T = \mathbf{0}$, the following Lyapunov candidate function is considered:

$$V = \frac{1}{2}\tilde{\mathbf{x}}^T\tilde{\mathbf{x}} \tag{6}$$

and its derivative along the system's trajectories

$$\dot{V} = \tilde{\mathbf{x}}^T\dot{\tilde{\mathbf{x}}} = \tilde{\mathbf{x}}^T(-\mathbf{K_s}\tanh(\mathbf{K}\tilde{\mathbf{x}}) + \boldsymbol{\delta}). \tag{7}$$

The following condition is obtained to ensure that $\dot{V}$ is negative definite:

$$|\tilde{\mathbf{x}}^T\mathbf{K_S}\tanh(\mathbf{K}\tilde{\mathbf{x}})| > |\tilde{\mathbf{x}}^T\boldsymbol{\delta}|. \tag{8}$$

Next, (8) is studied in a single dimension ($\tilde{x}$) to simplify the analysis. A similar study can be done with $\tilde{y}$, $\tilde{z}$, and $\tilde{\psi}$.

For large values of $\tilde{x}$, condition (8) can be reinforced as

$$|k'\tilde{x}| > |\delta_x\tilde{x}| \tag{9}$$

where $k' = k_{\mathrm{sx}}\tanh(k_x\tilde{x}_{\mathrm{aux}})$ and $\tilde{x}_{\mathrm{aux}}$ is the minimum value at which the error can be considered large. Thus, one condition for $\dot{V}$ to be negative definite is

$$k_{\mathrm{sx}} > \frac{|\delta_x|}{|\tanh(k_x\tilde{x}_{\mathrm{aux}})|}. \tag{10}$$

Condition (10) establishes a design parameter to guarantee that error $\tilde{x}$ will decrease.

Now, for the small values of $\tilde{x}$ ($\tilde{x} < \tilde{x}_{\mathrm{aux}}$), the condition given by (8) would be satisfied if

$$\left|\frac{k'}{\tilde{x}_{\mathrm{aux}}}\tilde{x}^2\right| > |\delta_x\tilde{x}|. \tag{11}$$

Meaning that a sufficient condition for $\dot{V}$ to be negative definite is

$$|\tilde{x}| > \frac{|\delta_x||\tilde{x}_{\mathrm{aux}}|}{|k_{\mathrm{sx}}\tanh(k_x\tilde{x}_{\mathrm{aux}})|} \tag{12}$$

implying that error $\tilde{x}$ is ultimately bounded by

$$|\tilde{x}| \leq \frac{|\delta_x||\tilde{x}_{\mathrm{aux}}|}{|k_{\mathrm{sx}}\tanh(k_x\tilde{x}_{\mathrm{aux}})|}. \tag{13}$$

Then, after the transient, $\tilde{\mathbf{x}}$ will be small ($\mathbf{K_s}\tanh(\mathbf{K}\tilde{\mathbf{x}}) \approx \mathbf{K_s}\mathbf{K}\tilde{\mathbf{x}}$), with error $\tilde{y}$, $\tilde{z}$, and $\tilde{\psi}$ bounds similar to (13).

Now, it is proved by contradiction that these control errors tend to zero.

The closed-loop equation (5) can be written after the transient as $\dot{\tilde{\mathbf{x}}} + \mathbf{K_s}\mathbf{K}\tilde{\mathbf{x}} = \boldsymbol{\delta}$ or, in Laplace transform form

$$\tilde{\mathbf{x}}(s) = (s\mathbf{I} + \mathbf{K_s}\mathbf{K})^{-1}\boldsymbol{\delta}(s). \tag{14}$$

According to (14) and recalling that $\mathbf{K_s}$ and $\mathbf{K}$ are positive constant diagonal matrices, the control error vector $\tilde{\mathbf{x}}$ and velocity difference vector $\boldsymbol{\delta}$ cannot be orthogonal. Nevertheless, both the vectors are orthogonal by definition (see *Remark* 1 and the minimum-distance criterion for $\mathbf{x_r}$ on P). Therefore, the only solution for steady state is that $\tilde{\mathbf{x}}(t) \to \mathbf{0}$ asymptotically [condition 1)], and, consequently, $V_a(t) \to V_d(t)$ [condition 2)]. □

Theorem 2: Let us consider the proposed control law (2) in closed loop with the quadrotor model (1). Then, if there is no perfect velocity tracking with bounded velocity error defined as $\tilde{\mathbf{u}} = \mathbf{u_c} - \mathbf{u}$, the error vector $\tilde{\mathbf{x}}$ is ultimately bounded.

Proof: Disregarding the assumption of perfect velocity tracking, (5) can now be written as

$$\dot{\tilde{\mathbf{x}}} + \mathbf{K_s}\tanh(\mathbf{K}\tilde{\mathbf{x}}) = \mathbf{J}\tilde{\mathbf{u}} + \boldsymbol{\delta}. \tag{15}$$

A Lyapunov candidate function (6) is considered, whose time derivative on the system's trajectories is

$$\dot{V} = \tilde{\mathbf{x}}^T(\mathbf{J}\tilde{\mathbf{u}} + \boldsymbol{\delta}) - \tilde{\mathbf{x}}^T\mathbf{K_s}\tanh(\mathbf{K}\tilde{\mathbf{x}}). \tag{16}$$

A sufficient condition for $\dot{V}$ to be negative definite is

$$|\tilde{\mathbf{x}}^T\mathbf{K_S}\tanh(\mathbf{K}\tilde{\mathbf{x}})| > |\tilde{\mathbf{x}}^T(\mathbf{J}\tilde{\mathbf{u}} + \boldsymbol{\delta})|. \tag{17}$$

Analyzing (17), following a similar analysis to the one made to condition (8), it can be concluded that, if:

$$k_{\mathrm{sx}} > \frac{|(\cos(\psi_a)\tilde{v}_{\mathrm{axc}} - \sin(\psi_a)\tilde{v}_{\mathrm{ayc}})||\delta_x|}{|\tanh(k_x\tilde{x}_{\mathrm{aux}})|} \tag{18}$$

the error $\tilde{x}$ will be ultimately bounded by

$$|\tilde{x}| \leq \frac{|(\cos(\psi_a)\tilde{v}_{\mathrm{axc}} - \sin(\psi_a)\tilde{v}_{\mathrm{ayc}})||\delta_x||\tilde{x}_{\mathrm{aux}}|}{|k_{\mathrm{sx}}\tanh(k_x\tilde{x}_{\mathrm{aux}})|}. \tag{19}$$

An equivalent analysis for errors $\tilde{y}$, $\tilde{z}$, and $\tilde{\psi}$ can be done to (17) to conclude that $\tilde{\mathbf{x}}$ is ultimately bounded. □

IV. Path Curvature and Quadrotor Speed

Using an intuitive analysis, it can be said that curvature measures what is missing from a curve to be a straight line at each point and gives a quantitative idea of the geometrical requirements of the path to be followed. By considering the required path r as a set of points, it is possible to know the value of curvature through

$$\Gamma(t) = \frac{|\dot{\mathbf{r}}(t) \times \ddot{\mathbf{r}}(t)|}{|\dot{\mathbf{r}}(t)|^3}. \tag{20}$$

However, to find the curvature value for a given path using (20), it is necessary to know the path analytical expression, which is not always available. For this reason, it is proposed to use an approximation instead of (20).

A. Approximation for the Path Curvature

Consider any path $P \in \Re^3$ represented by a set of equidistant points, and$\mathbf{p_1} = (x_1, y_1, z_1)$ and $\mathbf{p_2} = (x_2, y_2, z_2)$, two points contained in P separated by a small distance; $\boldsymbol{\nu_1}$ and $\boldsymbol{\nu_2}$ represent the path tangent vector in $\mathbf{p_1}$ and $\mathbf{p_2}$, respectively. Now, instead of calculating the angular difference between $\boldsymbol{\nu_1}$ and $\boldsymbol{\nu_2}$ in reference to a horizontal fixed reference, it is proposed to refer vector $\boldsymbol{\nu_2}$ to vector $\boldsymbol{\nu_1}$. Thus, the sought angle variation of the path direction is directly the angle between these two vectors $\boldsymbol{\nu_1}$ and $\boldsymbol{\nu_2}$.

If $\boldsymbol{\nu_1}$ and $\boldsymbol{\nu_2}$ are now unit vectors in spherical coordinates: $\boldsymbol{\nu_1} = [\cos\alpha_1\cos\beta_1\ \cos\alpha_1\sin\beta_1\ \sin\alpha_1]^T$ and $\boldsymbol{\nu_2} = [\cos\alpha_2\cos\beta_2\ \cos\alpha_2\sin\beta_2\ \sin\alpha_2]^T$; and recalling the definitions of scalar and dot products

$$\begin{aligned} \|\boldsymbol{\nu_1} \times \boldsymbol{\nu_2}\| &= \|\boldsymbol{\nu_1}\|\|\boldsymbol{\nu_2}\|\sin\gamma \\ \langle\boldsymbol{\nu_1} \cdot \boldsymbol{\nu_2}\rangle &= \|\boldsymbol{\nu_1}\|\|\boldsymbol{\nu_2}\|\cos\gamma \end{aligned} \tag{21}$$

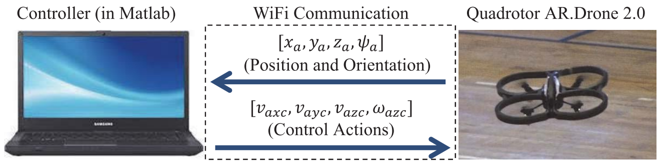

Fig. 3. Communication between quadrotor AR. Drone 2.0 and control PC.

where γ is the angle between both vectors or the change of the path direction between $\mathbf{p_1}$ and $\mathbf{p_2}$.

If γ is directly obtained from either of the two expressions in (21), singularities occur when the angle exceeds the value π. To avoid this problem, the following relationship is proposed:

$$\frac{\sin\gamma}{\cos\gamma} = \frac{\|\boldsymbol{v_1} \times \boldsymbol{v_2}\|}{\langle \boldsymbol{v_1} \cdot \boldsymbol{v_2}\rangle} \Rightarrow \gamma = \operatorname{atan2}(\|\boldsymbol{v_1} \times \boldsymbol{v_2}\|, \langle \boldsymbol{v_1} \cdot \boldsymbol{v_2}\rangle).$$

Then, the curvature can be approximated by $\Gamma = ((\gamma)/(\Delta l))$. The term Δl represents the distance between points $\mathbf{p_1}$ and $\mathbf{p_2}$. Note that when using this approximation, the points $\mathbf{p_i}$ must be equidistant along the entire path and the error in the approximation decreases as the points are closer to each other.

B. Quadrotor Speed Profile

Once the curvature of the path at each point is obtained, the proposed desired speed V_d for the kinematic controller is

$$V_d = f(V_{\max}, \Gamma) = \frac{V_{\max}}{1 + k_{\mathrm{sc}} \tanh(k_c |\Gamma(i+N)|)} \tag{22}$$

where k_{sc} and k_c are positive tuning parameters that set the minimum value of V_d and the hyperbolic tangent mapping; $V_{\max}$ is the maximum speed at which the aircraft can navigate (in terms of its physical limitations and the application). According to (22), the reference speed decreases in curved path and increases in straight parts. This variation is modulated by the geometric requirements of the path and parameters k_c and k_{sc}. This way, $\tilde{\mathbf{x}}$ decreases.

Since the path is known, it is possible to use the value of curvature N-points forward (prediction) to attenuate the desired speed with anticipation and allow the low-level control to react properly in time; this is done modifying the design parameter N. Thus, the proposed speed is bounded between

$$\frac{V_{\max}}{1 + k_{\mathrm{sc}}} \le V_d \le V_{\max}. \tag{23}$$

V. Coupling the Kinematic Controller to the Quadrotor

To test the kinematic controller in a real quadrotor AR. Drone 2.0, the control law is programmed in a computer in MATLAB environment. The computer communicates with the quadrotor through a WiFi network and the data exchange is possible using a dedicated software application interfacing MATLAB and the quadrotor.[2] Hence, control actions are sent to the quadrotor, whereas position, orientation, and velocities are received from it (Fig. 3).

[2] A C++ program working as a proxy using shared memory, based on the CV Drone project (https://github.com/puku0x/cvdrone), has been developed to communicate MATLAB with the AR. Drone 2.0.

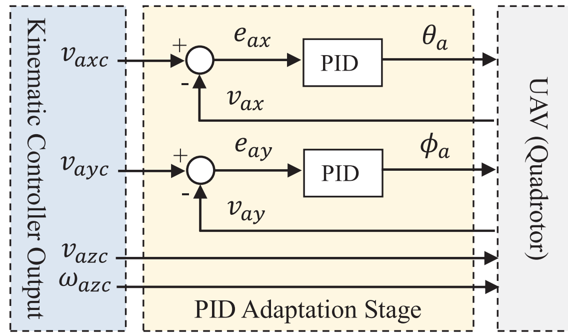

Fig. 4. Adaptation of the kinematic controller to the dynamic model of the quadrotor.

The speed in both the x and y axes (v_{ax}, v_{ay}) delivered by the quadrotor are in the reference frame attached to it; so, in order to express them in the inertial frame ($\dot{x}_a$, $\dot{y}_a$), the rotation matrix $\mathbf{J}$ must be used. This way, the aircraft position (x_a, y_a) is obtained by integrating the rotated speeds. Position in the z-axis z_a and yaw angle ψ_a are directly obtained from the onboard sensors (ultrasonic, accelerometers, and gyroscopes).

Then, the proposed kinematic controller calculates the speeds $\mathbf{u_c}$, allowing the quadrotor to follow the path of interest, as indicated in (2):

$$\mathbf{u_c} = \mathbf{J}^{-1}[\mathbf{K_s} \tanh(\mathbf{K}\tilde{\mathbf{x}}) + \mathbf{v_d}]$$

$$\begin{bmatrix} v_{\mathrm{axc}} \\ v_{\mathrm{ayc}} \\ v_{\mathrm{azc}} \\ \omega_{\mathrm{azc}} \end{bmatrix} = \mathbf{J}^{-1} \begin{bmatrix} k_{\mathrm{sx}} \tanh(k_x \tilde{x}) + V_d \cos(\varphi_r)\cos(\theta_r) \\ k_{\mathrm{sy}} \tanh(k_y \tilde{y}) + V_d \cos(\varphi_r)\sin(\theta_r) \\ k_{\mathrm{sz}} \tanh(k_z \tilde{z}) + V_d \sin(\varphi_r) \\ k_{s\psi} \tanh(k_\psi \tilde{\psi}) \end{bmatrix}.$$

While speeds v_{azc} and ω_{azc} can be sent directly to the quadrotor low-level controller, speeds v_{axc} and v_{ayc} must be converted to pitch (θ_a) and roll (ϕ_a) angle commands, respectively. For this reason, two PID controllers are incorporated in the output of the kinematic controller to generate θ_a and ϕ_a depending on the x-axis (e_{ax}) and y-axis (e_{ay}) speed errors, respectively. This is shown in Fig. 4.

Fig. 4 exposes the flexibility of this kinematic-based controller. Modifying only the adaptation stage, it is possible to use the same controller for other types of miniature rotorcraft, e.g., using the "inner-loop controller" of [26] as an adaptation stage, the path-following control can be applied to a miniature helicopter; however, the speed profile must be analyzed and suitably chosen for each particular case.

VI. Experimental Results

This section summarizes the main experimental results. Hereinafter, in Figs. 6–8, the red (or gray) line is the reference and the black lines are the quadrotor actual values. The kinematic controller's constants are: $k_x = k_z = 1.6$, $k_y = 1.4$, $k_\psi = 1.8$, and $k_{\mathrm{si}} = 1.5$ (where $i = x, y, z, \psi$). The value of N depends on how quickly the low-level control of the quadrotor can achieve the desired speed. In this brief, $N = 0$ is adopted, since this is the worst case scenario. All experiments were performed in a closed environment in order to obtain good results for comparison by avoiding windy conditions. Moreover, in all the cases, the same set of batteries mentioned in Section II were used initially with full load.

TABLE II
ELLIPTICAL PATH AND 80 s OF NAVIGATION

$V_d[m/s]$	**RMSE** $[m]$	**TD** $[m]$	**Consumed Energy** $[\%]$
1.5	0.31	116	13
$f(V_{max}, \Gamma)$	0.3	160	13.5

A radio control is employed with two objectives: first, to bring the UAV to a desired starting position and second, to enable an emergency landing.

Two types of experiments were proposed: 1) fixed time navigation and 2) fixed distance navigation.

A. Experiment at Fixed Time

In this case, the reference is an elliptical path at a constant height of 1 m and radius $a = 8$ and $b = 4$. The quadrotor navigates over this path for a fixed time of 80 s under different desired velocities, then, the root-mean-square position error (RMSE) and the traveled distance (TD) are calculated with the purpose to obtain a conclusion in reference to energy saving.

In the first place, the variable speed reference profile is considered (22) with the following parameters: $k_{\text{sc}} = 2$, $k_c = 0.8$, and $V_{\max} = 2$. Now, the objective is to find a constant speed ($V_d = \text{cte}$) to obtain the same RMSE (for the same path and time). This velocity is $V_d = 1.5$ m/s. After that, once the same battery is charged back to full load, the experience is repeated for 80 s and the results are summarized in Table II. In the following link, there is a video of this experience: https://youtu.be/pJdsENRm9Uc.

These results can be interpreted in two ways: 1) for the same position error, 36% of extra path can be covered using the proposed speed given by (22) (V_d as a function of the curvature) or 2) for the same position error, the distance of 116 m could be flown with less energy using (22).

Fig. 5 shows the reference path and orientation and the actual position x_a, y_a, z_a and orientation ψ_a of the quadrotor. Once the quadrotor reaches the path, control errors diminish considerably and remain bounded, reaffirming the theoretical results of Section III-B. Fig. 6 shows the control actions of the kinematic controller ($v_{\text{axc}}, v_{\text{ayc}}, v_{\text{azc}}, \omega_{\text{azc}}$), the actual quadrotor speeds ($v_{\text{ax}}, v_{\text{ay}}, v_{\text{az}}, \omega_{\text{az}}$), and V_a.

To test the controller in a more demanding path in terms of the curvature, the following hyperelliptical reference path is considered: $x(\theta) = \pm a \cos^{(2/n)} \theta$, $y(\theta) = \pm b \sin^{(2/n)} \theta$, $z = c$, where $0 \le \theta < (\pi/2)$, $a = b = 6$, $c = 1.8$, and $n = 4$. The path is approximately a square figure of 6 m × 6 m, at a fixed height of 1.8 m, and it is established that the quadrotor navigates over this path for a fixed time of 180 s. First, the path is traversed at different constant reference speeds of 1, 2, and 3 m/s, with three identical fully charged batteries in each case. After that, the same path is traversed at variable speed as a function of the curvature (with $V_{\max} = 3$ m/s, $k_{\text{sc}} = 2$, and $k_c = 0.8$; thus, the desired speed along the path has a value between $3 > V_d > 1.4$ m/s). In all the cases, the RMSE and the amount of travel distance have been considered.

Fig. 7 shows the reference path and the actual position x_a, y_a, z_a of the quadrotor for each speed reference. Fig. 8 shows the control actions of the kinematic controller for V_d

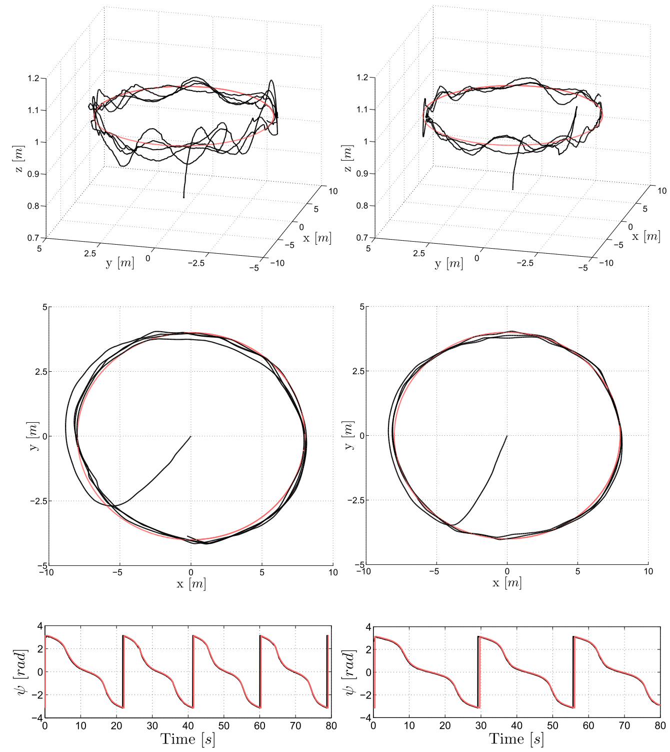

Fig. 5. Trajectory (3-D and XY views) and the orientation of the aircraft with $V_d = f(V_{\max}, \Gamma)$ (at the left) and $V_d = \text{cte} = 1.5$ m/s (at the right).

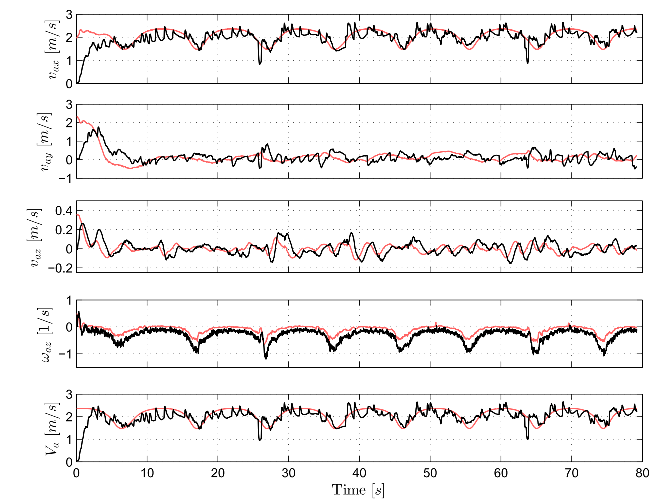

Fig. 6. Reference and actual speeds of the quadrotor, $V_d = f(V_{\max}, \Gamma)$ with $V_{\max} = 3$ m/s. Elliptical path reference.

as a function of the curvature, where it is possible to observe that the quadrotor speed during cornering decreases to a value of 1.4 m/s and tends to $V_{\max}$ in straight sections of the path. In the case where the constant reference speed is 3 m/s, the quadrotor fails to follow the requested path, and it was forced to land; this can be seen in Fig. 7(c) and (g).

Table III shows the experimental results; there it is possible to note that for the same position error of 0.25 m approximately, a 12.5% (42 m) of extra path can be covered using the proposed speed given by (22). Even in this case, where the quadrotor faces important direction changes on numerous occasions (approximately 52 times) within a short period of time, satisfactory results are achieved. On the other hand, it can

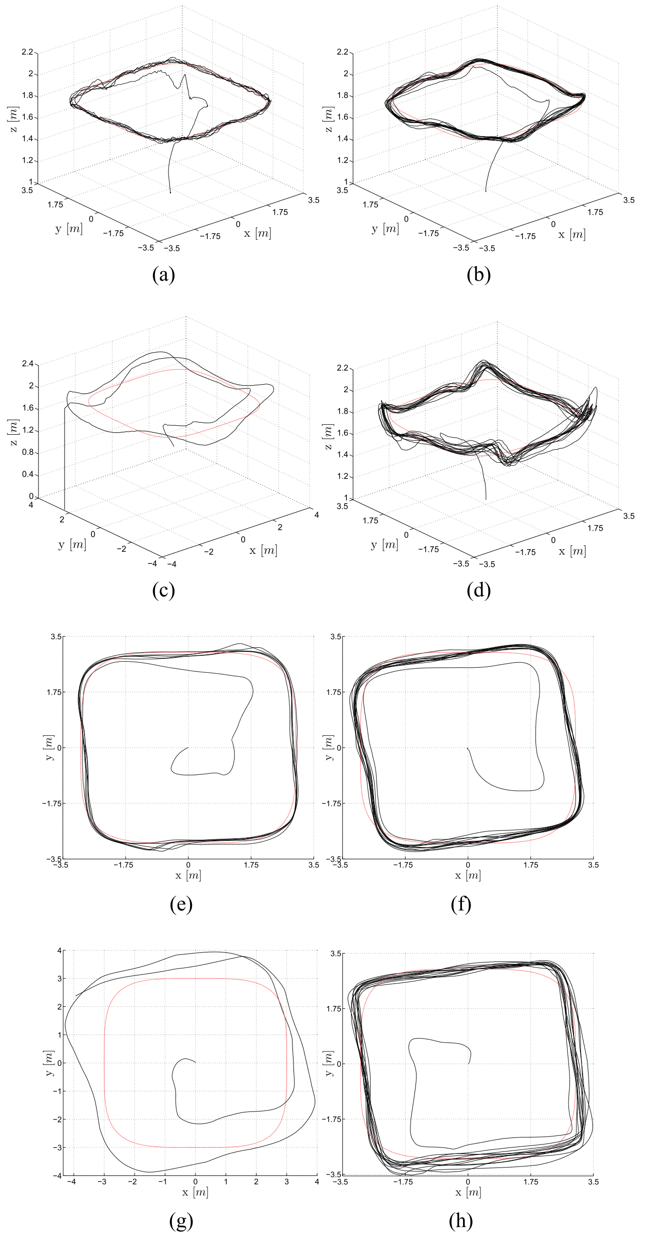

Fig. 7. 3-D views (top four) and XY views (bottom four) of reference and actual position of the quadrotor. (a) and (e) $\rightarrow$ V_d = cte = 1 m/s. (b) and (f) $\rightarrow$ V_d = cte = 2 m/s. (c) and (g) $\rightarrow$ V_d = cte = 3 m/s. (d) and (h) $\rightarrow$ $V_d = f(V_{\max}, \Gamma)$.

be seen that in all the cases, the power consumption is almost the same regardless of the speed. This is mainly because the aircraft was in the air during the same time in each experiment, which reinforces the experimental results of Section II.

The small oscillations along the z-axis (maximum 10%) observed in Figs. 5 and 7 when $V_d = f(V_{\max}, \Gamma)$ can be reduced adjusting N (22) in order for the quadrotor to slow down its velocity, modifying the desired speed (V_d) before entering the curve. A more adequate low-level control on board the quadrotor, e.g., using a more accurate distance sensor, would also help to reduce these oscillations.

B. Experiment at Fixed Distance

Finally, the first experiment is repeated (elliptical path), but this time until a fixed TD of 500 m is achieved. At the end of each experiment, the energy consumption is considered. Table IV resumes the results indicating that for approximately equal position error, the distance of 500 m could be flown saving 25% energy when using V_d as a function of the curvature.

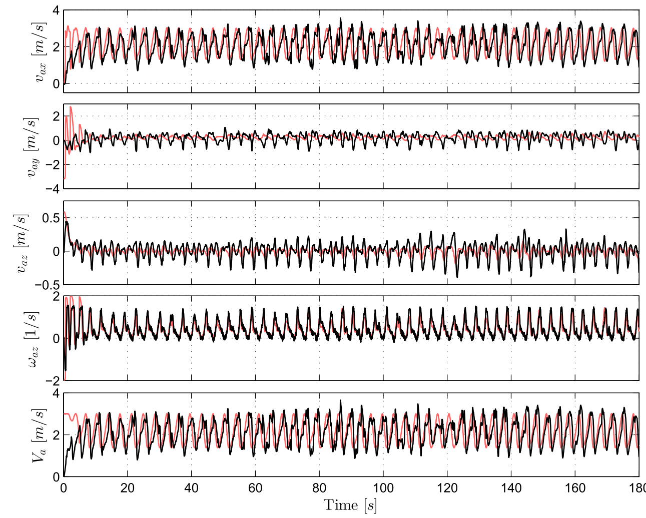

Fig. 8. Reference and actual speeds of the quadrotor, $V_d = f(V_{\max}, \Gamma)$ with $V_{\max} = 3$ m/s. Hyperelliptical path reference.

TABLE III

HYPERELLIPTICAL PATH AND 180 s OF NAVIGATION

$V_d [m/s]$	**RMSE** $[m]$	**TD** $[m]$	**Consumed Energy** $[\%]$
1	0.19	176	33.5
2	**0.25**	340	34.5
3	1.25	-	-
$f(V_{max}, \Gamma)$	**0.26**	382	33

TABLE IV

ELLIPTICAL PATH AND A FIXED DISTANCE OF 500 m

$V_d [m/s]$	**RMSE** $[m]$	**TD** $[m]$	**Consumed Energy** $[\%]$
1.5	0.124	500	81
$f(V_{max}, \Gamma)$	0.13	500	56

VII. DISCUSSION

Analyzing the experimental procedure and results summarized in Tables I–IV, some notes can be made.

1) Although navigation speeds were low, limited by the vehicle instability and indoor environment size, they represent an important part of the practical (secure) flight envelope of miniature rotorcrafts, especially in autonomous missions. However, we plan to obtain further experimental results with a more robust and higher thrust-to-weight ratio quadrotor and work in the development of a new mathematical model of the rotorcraft energy performance to correlate these results.
2) The energy consumption in the experiments with fixed time was about the same for different velocity profiles. These results indicate that less control efforts, whether they are velocities or accelerations, do not necessarily translate into real-world energy savings.
3) It is well known that flying style can affect power consumption and reduce flight time, e.g., flying aggressively

or making aerobatic maneuvers. Nevertheless, it seems that the most energy-efficient way for a quadrotor to follow a certain path is flying as fast as possible within its flight envelope and acceptable error margins. In the context of optimal control theory, this would mean that a time-optimal solution is also energy optimal. More research is needed to explore this issue in greater depth.

4) Ideally, with very accurate models of the rotorcraft, battery, and environment, a time-energy optimal control could be applied to follow a predefined path. This is a well-established result in optimal control theory applied to robotics [28], [29].

VIII. Conclusion

This brief proposed a stable path-following controller based on the simplified kinematic model of a quadrotor. Several experiments have been carried out showing the suitable performance of this controller under constant and variable desired speed profiles. The proposed variable speed profile is defined by the geometric requirements of the predetermined path. The percentages of the remaining battery load after each trial can be known due to the inclusion of the LiPo battery model. This allowed to conclude about the energy savings introduced by acting only over the desired velocity. The stability of the kinematic controller has been demonstrated using the Lyapunov theory, and its coupling to the dynamic model of a real quadrotor has been explained. This way, by only modifying the adaptation stage, the same kinematic controller can be used in other rotorcraft UAVs.

The experimental results in a real quadrotor show the good performance of the proposed controller and energy saving achieved. Two types of experiments were performed: one for fixed time and another for fixed distance. In the first case, it is reported how, for the same position error, an average of 24% of extra path can be covered using the proposed variable speed control law. In the second case, it is reported how, for almost the same position error, the 500 m distance is flown using 25% less energy, while using the same strategy.

Hopefully, this information will be helpful for decision makers in relation to the viability of using miniature rotorcraft UAVs for missions with limited energetic autonomy.

References

[1] S. Omari, M.-D. Hua, G. Ducard, and T. Hamel, "Hardware and software architecture for nonlinear control of multirotor helicopters," *IEEE/ASME Trans. Mechatronics*, vol. 18, no. 6, pp. 1724–1736, Dec. 2013.

[2] J. Jiang, J. Qi, D. Song, and J. Han, "Control platform design and experiment of a quadrotor," in *Proc. 32nd Chin. Control Conf. (CCC)*, Jul. 2013, pp. 2974–2979.

[3] I. Tjernberg, J. Lindberg, and K. Hansson, "Cooperative networked control of unmanned air vehicles," Bachelor's Degree Project, Dept. Electr. Eng., KTH Roy. Inst. Technol., Stockholm, Sweden, 2011.

[4] A. P. Aguiar, J. P. Hespanha, and P. V. Kokotović, "Path-following for nonminimum phase systems removes performance limitations," *IEEE Trans. Autom. Control*, vol. 50, no. 2, pp. 234–239, Feb. 2005.

[5] B. Erginer and E. Altuğ, "Design and implementation of a hybrid fuzzy logic controller for a quadrotor VTOL vehicle," *Int. J. Control, Autom. Syst.*, vol. 10, no. 1, pp. 61–70, 2012.

[6] M. Abdolhosseini, Y. M. Zhang, and C. A. Rabbath, "An efficient model predictive control scheme for an unmanned quadrotor helicopter," *J. Intell. Robot. Syst.*, vol. 70, nos. 1–4, pp. 27–38, 2013.

[7] H. Boudjedir, O. Bouhali, and N. Rizoug, "Neural network control based on adaptive observer for quadrotor helicopter," *Int. J. Inf. Technol., Control Autom.*, vol. 2, no. 3, pp. 39–54, 2012.

[8] J. Wu, H. Peng, Q. Chen, and X. Peng, "Modeling and control approach to a distinctive quadrotor helicopter," *ISA Trans.*, vol. 53, no. 1, pp. 173–185, 2014.

[9] Z. T. Dydek, A. M. Annaswamy, and E. Lavretsky, "Adaptive control of quadrotor UAVs: A design trade study with flight evaluations," *IEEE Trans. Control Syst. Technol.*, vol. 21, no. 4, pp. 1400–1406, Jul. 2013.

[10] A. S. Brandão, D. Gandolfo, M. Sarcinelli-Filho, and R. Carelli, "PVTOL maneuvers guided by a high-level nonlinear controller applied to a rotorcraft machine," *Eur. J. Control*, vol. 20, no. 4, pp. 172–179, 2014.

[11] J.-J. Xiong and E.-H. Zheng, "Position and attitude tracking control for a quadrotor UAV," *ISA Trans.*, vol. 53, no. 3, pp. 725–731, 2014.

[12] C. Rosales, D. Gandolfo, G. Scaglia, M. Jordan, and R. Carelli, "Trajectory tracking of a mini four-rotor helicopter in dynamic environments—A linear algebra approach," *Robotica*, vol. 33, no. 8, pp. 1628–1652, 2015.

[13] A. Akhtar, S. L. Waslander, and C. Nielsen, "Path following for a quadrotor using dynamic extension and transverse feedback linearization," in *Proc. IEEE Conf. Decision Control*, Dec. 2012, pp. 3551–3556.

[14] D. Cabecinhas, R. Cunha, and C. Silvestre, "Rotorcraft path following control for extended flight envelope coverage," in *Proc. IEEE Conf. Decision Control*, Dec. 2009, pp. 3460–3465.

[15] S. Zeghlache, D. Saigaa, K. Kara, A. Harrag, and A. Bouguerra, "Backstepping sliding mode controller improved with fuzzy logic: Application to the quadrotor helicopter," *Arch. Control Sci.*, vol. 22, no. 3, pp. 315–342, 2012.

[16] A. Hernandez, C. Copot, R. De Keyser, T. Vlas, and I. Nascu, "Identification and path following control of an AR.Drone quadrotor," in *Proc. IEEE 17th Int. Conf. Syst. Theory, Control Comput. (ICSTCC)*, Oct. 2013, pp. 583–588.

[17] D. Zhou and M. Schwager, "Vector field following for quadrotors using differential flatness," in *Proc. IEEE Int. Conf. Robot. Autom.*, May/Jun. 2014, pp. 6567–6572.

[18] Y. M. Zhang *et al.*, "Development of advanced FDD and FTC techniques with application to an unmanned quadrotor helicopter testbed," *J. Franklin Inst.*, vol. 350, no. 9, pp. 2396–2422, 2013.

[19] C. Papachristos, K. Alexis, and A. Tzes, "Linear quadratic optimal trajectory-tracking control of a longitudinal thrust vectoring-enabled unmanned Tri-TiltRotor," in *Proc. IEEE Annu. Conf. Ind. Electron. Soc. (IECON)*, Nov. 2013, pp. 4174–4179.

[20] D. Cabecinhas, R. Naldi, L. Marconi, C. Silvestre, and R. Cunha, "Robust take-off for a quadrotor vehicle," *IEEE Trans. Robot.*, vol. 28, no. 3, pp. 734–742, Jun. 2012.

[21] M. Ryll, H. H. Bülthoff, and P. R. Giordano, "Modeling and control of a quadrotor UAV with tilting propellers," in *Proc. IEEE Int. Conf. Robot. Autom.*, May 2012, pp. 4606–4613.

[22] L. R. G. Carrillo, A. Dzul, and R. Lozano, "Hovering quad-rotor control: A comparison of nonlinear controllers using visual feedback," *IEEE Trans. Aerosp. Electron. Syst.*, vol. 48, no. 4, pp. 3159–3170, Oct. 2012.

[23] A. Kalantari and M. Spenko, "Design and experimental validation of HyTAQ, a hybrid terrestrial and aerial quadrotor," in *Proc. IEEE Int. Conf. Robot. Autom.*, May 2013, pp. 4445–4450.

[24] D. Gandolfo, A. Brandão, D. Patiño, and M. Molina, "Dynamic model of lithium polymer battery—Load resistor method for electric parameters identification," *J. Energy Inst.*, vol. 88, no. 4, pp. 470–479, 2014.

[25] M. Bangura and R. Mahony, "Nonlinear dynamic modeling for high performance control of a quadrotor," in *Proc. Austral. Conf. Robot. Autom.*, 2012, pp. 1–10.

[26] L. R. Salinas, E. Slawiñski, and V. A. Mut, "Kinematic nonlinear controller for a miniature helicopter via Lyapunov techniques," *Asian J. Control*, vol. 16, no. 3, pp. 856–870, 2014.

[27] V. Andaluz, F. Roberti, J. M. Toibero, and R. Carelli, "Adaptive unified motion control of mobile manipulators," *Control Eng. Pract.*, vol. 20, no. 12, pp. 1337–1352, 2012.

[28] J. E. Bobrow, S. Dubowsky, and J. S. Gibson, "Time-optimal control of robotic manipulators along specified paths," *Int. J. Robot. Res.*, vol. 4, no. 3, pp. 3–17, Sep. 1985.

[29] Z. Shiller, "Time-energy optimal control of articulated systems with geometric path constraints," *J. Dyn. Syst., Meas., Control*, vol. 118, no. 1, pp. 139–143, 1996.